European Journal of Pharmaceutics and Biopharmaceutics 95 (2015) 368–377

Contents lists available at ScienceDirect

European Journal of Pharmaceutics and Biopharmaceutics

journal homepage: www.elsevier.com/locate/ejpb

Research Paper

Sunitinib microspheres based on [PDLLA-PEG-PDLLA]-*b*-PLLA multi-block copolymers for ocular drug delivery

F. Ramazani [a,b], C. Hiemstra [c], R. Steendam [c], F. Kazazi-Hyseni [a], C.F. Van Nostrum [a], G. Storm [a,d], F. Kiessling [b], T. Lammers [b,d], W.E. Hennink [a], R.J. Kok [a,*]

[a] Department of Pharmaceutics, Utrecht Institute for Pharmaceutical Sciences, Utrecht University, The Netherlands
[b] Department of Experimental Molecular Imaging, RWTH-Aachen University, Aachen, Germany
[c] InnoCore Pharmaceuticals, Groningen, The Netherlands
[d] Department of Controlled Drug Delivery, University of Twente, The Netherlands

ARTICLE INFO

Article history:
Received 17 November 2014
Revised 5 February 2015
Accepted in revised form 9 February 2015
Available online 19 February 2015

Keywords:
Sunitinib malate
[PDLLA-PEG-PDLLA]-*b*-PLLA
Multi-block copolymers
Single emulsion (O/W)
Microspheres
Thermal analysis
Release and degradation
Angiogenesis
Ocular drug delivery

ABSTRACT

Sunitinib is a multi-targeted receptor tyrosine kinase (RTK) inhibitor that blocks several angiogenesis related pathways. The aim of this study was to develop sunitinib-loaded polymeric microspheres that can be used as intravitreal formulation for the treatment of ocular diseases. A series of novel multi-block copolymers composed of amorphous blocks of poly-(D,L-lactide) (PDLLA) and polyethylene glycol (PEG) and of semi-crystalline poly-(L-lactide) (PLLA) blocks were synthesized. Sunitinib-loaded microspheres were prepared by a single emulsion method using dichloromethane as volatile solvent and DMSO as co-solvent. SEM images showed that the prepared microspheres (~30 μm) were spherical with a non-porous surface. Sunitinib-loaded microspheres were studied for their degradation and *in-vitro* release behavior. It was found that increasing the percentage of amorphous soft blocks from 10% to 30% accelerated the degradation of the multi-block copolymers. Sunitinib microspheres released their cargo for a period of at least 210 days by a combination of diffusion and polymer erosion. The initial burst (release in 24 h) and release rate could be tailored by controlling the PEG-content of the multi-block copolymers. Sunitinib-loaded microspheres suppressed angiogenesis in a chicken chorioallantoic membrane (CAM) assay. These microspheres therefore hold promise for long-term suppression of ocular neovascularization.

1. Introduction

Vascular endothelial growth factor (VEGF) is a signaling protein that stimulates angiogenesis and vasculogenesis [1,2]. Overexpression of VEGF has been implicated as an essential factor promoting neovascularization and increasing vascular permeability in many ocular diseases including age-related macular degeneration (AMD), diabetic retinopathy and retinal vein occlusion [3–5]. Thus, VEGF represents a validated target for normalization of retinal vascularization [4,6,7]. Current treatments include the VEGF-neutralizing monoclonal antibody fragment ranibizumab and anti-VEGF RNA aptamer (pegaptanib) which have been approved by the FDA for the treatment of AMD [1,6,8]. Both treatments can slow down the progression of vision loss to some extent. However, further improvement in the treatment of ocular diseases is needed, preferably by agents with a sustained activity within the posterior segment of the eye. Sunitinib malate (Sutent) is a multi-targeted receptor tyrosine kinase (RTK) inhibitor which is approved by the FDA for the treatment of renal cell carcinoma and gastrointestinal stromal tumors [9,10]. Inhibition of VEGFRs using sunitinib efficiently suppressed the retinal neovascularization in a hypoxia-induced retinal angiogenesis zebra fish model [11]. In another study of Takahashi et al., oral administration of sunitinib was beneficial in treating an experimental choroidal neovascularization mice model [12]. Sunitinib, however, is associated with

Abbreviations: PLLA, poly(L-lactide); PDLA, poly(D,L-lactide; PEG, polyethylene glycol; M_w, weight average molecular weight; O/W, oil in water; LE, loading efficiency; LC, loading capacity; RO, reverse osmosis; T_g, glass transition temperature; T_m, melting temperature; ΔH_m, melting enthalpy; T_c, crystallization temperature; ΔH_c, crystallization enthalpy; SEM, scanning electron microscopy; DSC, differential scanning calorimetry; DCM, dichloromethane; DMSO, dimethyl sulfoxide; PVA, polyvinylalcohol; THF, tetrahydrofuran; PBS, phosphate buffered saline; TL, theoretical loading; GPC, gel permeation chromatography; MS, microspheres; CAM, chick embryo chorioallantoic membrane; M_n, number average molecular weight.

* Corresponding author. Department of Pharmaceutics, Utrecht Institute for Pharmaceutical Sciences, Utrecht University, Universiteitsweg 99, 3584 CG Utrecht, The Netherlands. Tel.: +31 620275995; fax: +31 30 251789.
E-mail address: r.j.kok@uu.nl (R.J. Kok).

http://dx.doi.org/10.1016/j.ejpb.2015.02.011
0939-6411/

dose-dependent adverse effects, ranging from mild fatigue and hand-foot syndrome to life-threatening cardiac toxicity [13–15]. Moreover, repeated and long-term intravitreal injections may cause problems, such as retinal detachment, vitreous hemorrhage, or endophthalmitis [16–18]. Therefore, we propose to deliver sunitinib locally in the eye by intravitreal injection of a depot preparation capable of sustained release. Development of a sustained release formulation of sunitinib using biodegradable microspheres can decrease the frequency of injections and lead to new regimens for the treatment of posterior eye diseases.

In the present study a series of novel multi-block copolymers (Fig. 1), consisting of rigid semi-crystalline poly(L-lactide) blocks (PLLA) and soft amorphous blocks containing poly(D,L-lactide) (PDLLA) and polyethylene glycol (PEG) (PDLLA-PEG-PDLLA) were synthesized and used to prepare sunitinib microspheres. By varying the composition of this type [PDLLA-PEG-PDLLA]-*b*-[PLLA] multi-block copolymers the hydrophilicity/hydrophobicity, glass transition temperature (T_g) as well as the degradation kinetics can be tailored [19–22], which allowed us to control the release kinetics of sunitinib. We further report on the anti-angiogenic effect of the sunitinib-loaded microspheres using a chick chorioallantoic membrane (CAM) assay.

2. Materials and methods

2.1. Materials

Sunitinib malate was obtained from LC laboratories, USA. Poly(vinyl alcohol) (PVA; M_w 30,000–70,000; 88% hydrolyzed), Tween 20, stannous octoate and dimethyl sulfoxide (DMSO) were obtained from Sigma Aldrich, Germany. Dichloromethane (DCM), acetonitrile and tetrahydrofuran (THF) were purchased from Biosolve (Valkenswaard, The Netherlands). PEG1000, 1,4-butanediol and 1,4 dioxane were purchased from Acros (Geel, Belgium), 1,4-butanediisocyanate was purchased from Bayer (Leverkusen, Germany) and DL-lactide and L-lactide were purchased from Corbion Purac (Gorinchem, The Netherlands). Polystyrene standards were purchased from Agilent technologies (Santa Clara, USA). Fertilized white Leghorn eggs were obtained from Het Anker company (Ochten, The Netherlands).

2.2. Synthesis of multi-block copolymers

[PDLA-PEG-PDLA]-*b*-[PLLA] multi-block copolymers with [PDLA-PEG-PDLA]/[PLLA] block ratios of 10/90, 20/80 and 30/70 w/w were synthesized and characterized using similar procedures as described previously [20]. In short, PDLLA-PEG-PDLLA and PLLA prepolymers were synthesized by standard stannous octoate catalyzed ring-opening polymerization. To prepare PDLLA-PEG-PDLLA with a target molecular weight of 2000 g/mol, D,L-lactide and PEG1000 were introduced into a three-necked bottle under nitrogen atmosphere and PEG1000 was added, followed by addition of the catalyst stannous octoate at a ratio of 12,350 mol/mol (monomer/catalyst). The weights of the materials are listed in Supplementary Table S1. The mixture was stirred for 189 h at 140 °C and subsequently cooled down to room temperature. The lactic acid/PEG (LA/PEG) composition of PDLLA-PEG-PDLLA prepolymer was characterized by ^{1}H NMR analysis as described in the Supplementary data (Supplementary Table S2).

PLLA prepolymer with a target molecular weight of 4000 g/mol, was synthesized by dissolution of L-lactide and 1,4-butanediol in 1,4-dioxane (distilled over sodium wire) after which stannous octoate was added at a ratio of 12,500 mol/mol (monomer/catalyst). The mixture was stirred at 90 °C and cooled down to room temperature when monomer conversion was $\sim\geqslant$95% (^{1}H NMR analysis). Supplementary Tables S3 and S4 list the weights of materials used for the synthesis of PLLA and ^{1}H NMR characterization of the PLLA prepolymer, respectively.

The PDLLA-PEG-PDLLA and PLLA prepolymers were chain-extended with 1,4-butanediisocyanate to prepare X[PDLLA-PEG-PDLLA]-*b*-Y[PLLA] multi-block copolymers with X/Y being 10/90, 20/80 and 30/70 w/w. PDLLA-PEG-PDLLA and PLLA prepolymers were introduced into a reactor under a nitrogen atmosphere. 1,4-Dioxane (distilled over sodium wire) was added to obtain a polymer concentration of 30% w/w and the mixture was heated to 80 °C to dissolve the prepolymers. Distilled 1,4-butanediisocyanate was added and the reaction mixture was stirred overnight, where after the reaction mixture was diluted with non-distilled dioxane, and cooled to room temperature. Finally, the reaction mixture was transferred into a tray and vacuum-dried at 30 °C. Supplementary Tables S5 and S6 list the weights of materials used for the synthesis of multi-block copolymers and ^{1}H NMR characterization of the final copolymers.

Gel permeation chromatography (GPC) was used to analyze the molecular weights of prepolymers and the final block copolymers. GPC was carried out on a Waters Alliance system, with a Waters 2695 separating module and a Waters 2414 Refractive Index detector. Two PL-gel 5 μm mixed-D columns fitted with a guard column (Polymer Labs, M_w range 0.2–400 kg/mol) were used. THF (1 ml/min) was used as mobile phase and calibration was done with polystyrene standards.

2.3. Preparation of sunitinib-loaded microspheres

Sunitinib-loaded microspheres were prepared using a single emulsion solvent evaporation technique O/W as described in the literature [23,24]. Briefly, 25 μl of a solution of sunitinib malate in DMSO (40 mg/ml) was added to 475 μl of DCM in which 200 mg polymer was dissolved. This solution was subsequently emulsified in 1 ml of buffer pH 9.0 (0.25 M Tris hydrochloride)

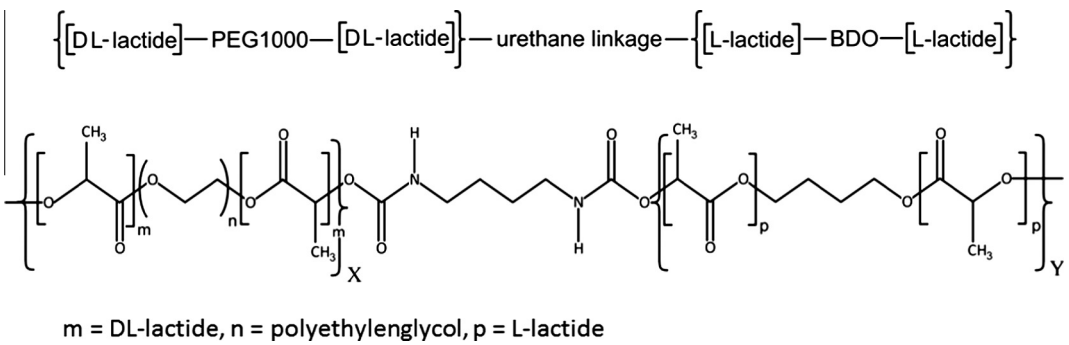

Fig. 1. The chemical structures of [PDLLA-PEG-PDLLA]-*b*-PLLA polymers used in this study. Polymer A (10% X, 90% Y), polymer B (20% X, 80% Y) and polymer C (30% X, 70% Y).

containing 1% PVA using an IKA homogenizer (IKA Labortechnik Staufen, Germany) for 30 s at maximum speed (30,000 rpm). The formed emulsion was subsequently transferred into 5 ml of the same PVA buffer and stirred using a magnetic stirrer (1000 rpm) at room temperature for 40 min. A possible concern of exposure of the microspheres to alkaline pH of the external aqueous phase is the OH-driven hydrolysis of the copolymers [25]. To minimize the exposure of microspheres to an aqueous solution of pH 9.0, the emulsion was then added to 44 ml buffer pH 7.0 (0.25 M sodium potassium phosphate buffer) containing 1% PVA and stirred at 500 rpm for 3 h. The formed microspheres were centrifuged (Laboratory centrifuge, 4 K 15 Germany) at 4000*g* for 3 min and washed two times with 100 ml 0.025% Tween 20 followed by two times washing with 100 ml reverse osmosis (RO) water and lyophilized. The obtained microspheres were stored at −20 °C. All the microsphere batches were prepared in triplicate.

2.4. Characterization of sunitinib-loaded microspheres

The average size and size distribution of the microspheres were measured using an Accusizer 780 (Optical particle sizer, Santa Barbara, California, USA). The volume weighted mean diameter (vol-wt mean) of the microspheres is reported as particle size. The morphology of the microspheres was studied by scanning electron microscopy (Phenom™, FEI Company, The Netherlands). Microspheres were glued on 12 mm diameter aluminum sample holders using conductive carbon paint (Agar scientific Ltd., England) and coated with palladium under vacuum using an ion coater.

The loading efficiency (LE) of sunitinib-loaded microspheres was determined by dissolving 5 mg of microspheres in DMSO and measuring the absorbance at 431 nm using an UV–vis spectrophotometer (Shimadzu uv-2450). Calibration was done with sunitinib dissolved in DMSO (concentration ranging from 5 to 40 μg/ml). LE of sunitinib in microspheres is reported as the amount of encapsulated drug divided by the amount of drug used for encapsulation. The non-encapsulated drug was also determined by measuring the amount of sunitinib in the external water phase after centrifugation of the microspheres using HPLC analysis [26]. Briefly, a gradient elution method was used with a mobile phase A (95% H_2O, 5% ACN and 0.1% TFA), a mobile phase B (95% ACN, 5% H_2O and 0.1% TFA) and a flow rate of 1 ml/min using a Sunfire™ C18 (5 μm) column. The eluent linearly changed from 5% to 95% ACN in 10 min; sunitinib retention time was at 7 min. Sunitinib standards (10 μl, 0.3–30 μg/ml PBS) were used for calibration and detection was done at 431 nm. Loading capacity (LC) is expressed as the encapsulated amount of sunitinib divided by the dry weight of the microspheres.

The microspheres yield is calculated as percentage of the weight of the obtained product divided by the initial weight of the solid materials.

Differential scanning calorimetry (DSC) analysis was done on a TA Instruments DSC Q2000 machine. Approximately 5 mg of freeze-dried microspheres was loaded into aluminum pans and the pans were closed. First, the samples were heated from 0 °C to 60 °C at a heating rate of 5 °C/min. Next, the samples were cooled down with the same rate to −20 °C or −80 °C and heated again to 220 °C with a rate of 2 °C/min and temperature modulation ±1 °C/30 s. The crystallization temperature (T_c) and melting temperature (T_m) were determined from the thermogram recorded in the second heating scan. The glass transition temperature (T_g) was determined from the thermogram of reverse heat flow.

X-ray diffraction (XRD) patterns were recorded for the polymers and drug-loaded microspheres using a Bruker X8-Proteum with Helios mirrors using CuKα radiation ($\lambda = 0.1.5418$ Å) on a Platinum-135 CCD detector. The patterns were recorded at a sample-to-detector distance of 60 mm. Separate blank patterns were recorded to allow subtraction of air and capillary wall-scattering. The two-dimensional X-ray scattered intensities were transformed into one-dimensional intensity with 2θ as the *x*-axis.

2.5. In-vitro degradation study of sunitinib-loaded microspheres

Samples of freeze-dried sunitinib-loaded microspheres (~10 mg) were transferred into Eppendorf tubes and dispersed in 1.5 ml of PBS (pH 7.4, 0.033 M NaH_2PO_4, 0.066 M Na_2HPO_4, 0.056 M NaCl) also containing 0.05% (w/w) NaN_3. The microsphere suspensions were incubated at 37 °C while gently shaking. Samples of microsphere dispersions (1.5 ml) were taken at predetermined time points, centrifuged and washed twice with 1 ml RO water and lyophilized. Dry masses were weighed and subsequently dissolved in THF (2 mg/ml) while gently shaking overnight. GPC-based analysis of the polymers as described above was used to analyze the change in polymer molecular weight during degradation. ^{1}H NMR analysis of the degraded microspheres dissolved in $CDCl_3$ (1 mg/ml) was performed using a Gemini-300 MHz spectrometer at 298 K. The weight percentage of PEG in degraded polymers was calculated from the methine group of polylactide at δ 5.4–5.1 and the methylene groups of PEG at δ 3.6–3.7.

2.6. In-vitro release of sunitinib-loaded microspheres

About 10 mg of sunitinib loaded microspheres were introduced into 2-ml Eppendorf tubes, and 1.5 ml of PBS (for the buffer composition see Section 2.5). The samples were incubated at 37 °C under mild agitation. Samples were collected at different time points after centrifugation by removing 1 ml of the supernatant and replacing it with 1 ml of fresh buffer. The collected supernatants were analyzed for released sunitinib using HPLC analysis as mentioned in Section 2.4.

In-vitro release data were fitted by linear and nonlinear regression analysis (Graphpad Prism version 4). Microspheres type A were fitted with either a linear zero-order release model (Eq. (1)), or an empirical model for sigmoidal drug release (Eq. (2)) according to Duvvuri et al. [27]. Microspheres type B and C were only fitted by the sigmoidal model.

$$Q = A + k * t \tag{1}$$

Q stands for cumulative drug release, *t* stands for the time since start of the release experiment, *A* = intercept with *Y*-axis (burst release); *k* = rate constant of release

$$Q = A * (1 - e^{-k_1 * t}) + \frac{B}{1 + e^{k_2 * (t - T_{50})}} \tag{2}$$

Q stands for cumulative drug release, *t* stands for the time since start of the release experiment, constants *A* and *B* stand for the relative fractions of initial release phase and late release phase, k_1 and k_2 represent the rate constants of the initial release phase and late release phase and T_{50} stands for the time to reach 50% of the drug release covered by the model.

2.7. Chick chorioallantoic membrane assay

Fertilized White Leghorn eggs were incubated at 37 °C and 60–65% relative humidity. After day 3 the eggs were candled and the positions of the embryo and air sac were marked. To disconnect the chick chorioallantoic membrane (CAM) from the shell, the area between the air sac and embryo was punctured using an 18 gouge needle and 2–3 ml of albumen (egg white) was removed. The holes were subsequently sealed using parafilm. At day seven of incubation, eggs were randomly divided into four groups, a small window (2 to 2 cm) was made using a scissors on the upper side of the egg

to get access to the CAM. To study the effect of sunitinib on the angiogenesis, nitrocellulose rings were applied on the top of the CAM. Next, using a sterile pipet, 30 μl of either vehicle (PBS), blank microspheres suspended in PBS (0.5 mg/egg), sunitinib solution in PBS (50 or 100 ng/egg) or sunitinib-loaded microspheres suspended in PBS (0.5 mg/egg corresponding to a total dose of 1350 ng sunitinib), prepared in aseptic condition, was applied onto the CAM. Pictures were taken using a digital camera before and 24 hours (h) after applying the drug and the number of blood vessels was counted. Statistical analysis was performed with GraphPad Prism software using paired Student's *t*-test by comparing the number of blood vessels before and 24 h after applying the drug.

3. Results and discussion

3.1. Physicochemical characteristics of the polymers

Table 1 shows the characteristics of the polymers and their building blocks (PEG1000, PDLLA-PEG-PDLLA and PLLA) that were used in this study. The molecular weight of the prepolymers and the final multi-block copolymers, as determined by GPC, are shown in Table 1. The number average molecular weight (M_n) of the PDLA-PEG-PDLA and PLLA prepolymers was 2000 and 4000 g/mol, respectively, while the average molecular weight (M_w) of multi-block copolymers was 37, 23 and 22 kg/mol for polymer A, B and C, respectively, confirming the successful chain-extension of the prepolymers. ^{1}H NMR was used to verify the overall lactate/PEG ratio of the final multi-block copolymers (Supplementary Table S6 and Fig. S1). The relative percentages of the buildings blocks were calculated from the methine group of polylactide at δ 5.4–5.1 and the $-CH_2CH_2-O$ methylene groups of PEG at δ 3.6–3.7, and enabled us to calculate the relative compositions of the block copolymers. The relative PEG content of the three polymers ranged from 4.8% w/w for polymer A, to 9.9% and 14.8% for polymer B and C, respectively. These percentages correlated closely to the initial weight percentages of the PDLA-PEG-PDLA and PLLA blocks (e.g. 10% in soft block, 90% in PLLA for polymer A).

Thermal analysis was done on both the prepolymers (building blocks) and on the final multi-block copolymers to understand their physical state (amorphous or semi-crystalline). DSC analysis starting at −80 °C showed that the PDLA-PEG-PDLA prepolymer had a T_g at −37 °C followed by an exothermic crystallization and melting endotherm at −2 °C and 10 °C, respectively (Fig. S2). Since the enthalpies of the observed melting and crystallization peaks were equal (ΔH_m and ΔH_c in Table 1), we concluded that PDLLA-PEG-PDLLA was fully amorphous at room temperature. This is in agreement with other studies in which PLA-PEG-PLA with LA/PEG ratios of more than 8 were also amorphous [28]. The observed T_g corresponded to the expected T_g according to Fox's equation [29], which confirmed the miscibility of the PEG and PDLLA blocks. Short chain PDLLA (T_g – 18 °C) [30] and PEG1000 (T_g – 41 °C) were used as reference.

The synthesized semi-crystalline PLLA showed a T_g of 45 °C, a T_m of 130 °C and a melting enthalpy of 46 (J/g) (Table 1 and Fig. S2). The percentage crystallinity of the PLLA prepolymer was 51%, which was calculated as follows:

$$\% \text{ crystallinity} = (\Delta H_m - \Delta H_c)/\Delta H_m^\circ * 100$$

where ΔH_m° is the heat of melting for 100% crystalline PLLA [30]. Similarly, the crystallinity of the final multi-block copolymers was calculated (Table 1). High molecular weight PLLA has a T_g of 60 °C, a melting temperature (T_m) of 170–180 °C and a melting enthalpy (ΔH_m) of 90 (J/g) [30,31].

A typical thermogram of the multi-block copolymers X[PDLLA-PEG-PDLLA]-*b*-Y[PLLA] is shown in Fig. 2. DSC analysis showed that the block copolymers A, B, and C had a T_g at 50 °C, 42 °C and 35 °C respectively, and also showed both crystallization (T_c at 85–91 °C) and melting (T_m at 131–137 °C) at higher temperatures. The crystallinity of the block copolymers was about 10–15%. Increasing the percentage of the soft block from 10% to 30% resulted in a decrease in the T_g of the final block copolymer from 50 °C to 35 °C which can be explained by the plasticizing effect of PEG on the amorphous PDLA/PLLA phase of the material [32]. The observed decrease in T_g for the copolymers corresponded to the expected changes in T_g according to Fox's equation using high molecular weight PLLA with a T_g of 60 °C as reference [30,31].

The physical state of the multi-block copolymers and their prepolymers was also studied by XRD crystallography. Fig. 3 shows the diffractograms of PEG1000, PLLA and the multi-block copolymers used in this study. XRD analysis of the PDLLA-PEG-PDLLA

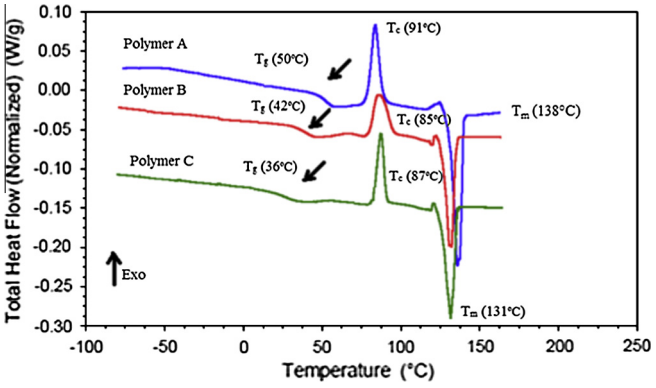

Fig. 2. Thermograms of multi-block copolymers utilized in this study (polymer A, B and C). (For the interpretation of the references to color in this figure legend, the reader is referred to the web version of this article.)

Table 1
Characteristics of the prepolymers and multi-block copolymers used in this study. A, B, and C are polymers utilized in the current study, PDLA-PEG-PDLA, PLLA and PEG1000 are the building blocks used for the synthesis of A, B and C.

(Pre-)polymer	M_w/M_n[a] (kg/mol)	PEG[b] (%)	T_g (°C)[c]	T_g (°C)[d]	ΔH_c[c] (J/g)	T_c[c] (°C)	ΔH_m[c] (J/g)	T_m[c] (°C)	C[e] (%)
PEG1000	1.3/1.1	100	−41	–	–		276	35	–
PDLLA-PEG-PDLLA	3.1/2.0	58	−37	−33	12	−2	13	10	0
PLLA	5.1/4.2	–	45	–	–	–	46	131	51
Block copolymer A	79/37	4.6	50	47	18	91	27	137	11
Block copolymer B	48/23	9.9	42	34	15	85	24	131	12
Block copolymer C	48/22	14.8	35	23	14	87	25	131	15

[a] Determined by GPC.
[b] Determined by ^{1}H NMR.
[c] Determined by DSC.
[d] T_g of the final multi-block copolymers as calculated by Fox equation using reference materials PLLA (T_g 60 °C) and PEG1000 (T_g – 41 °C).
[e] % of crystallinity = $(\Delta H_m - \Delta H_c)/\Delta H_m^\circ * 100$ where ΔH_m° is the heat of melting for 100% crystalline PLLA.

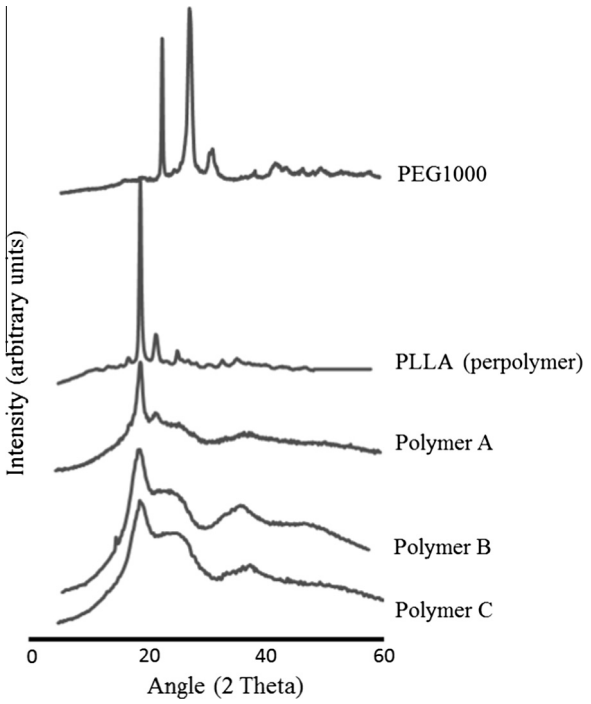

Fig. 3. The XRD patterns of PEG1000, PLLA (prepolymer), polymer A, polymer B and polymer C. Intensity scaling is arbitrarily applied to the curves.

prepolymer could not be performed as this product was a semi-solid material. The clear peaks in the diffractograms of PEG1000 and the PLLA prepolymer showed that these polymers were semi-crystalline, in agreement with DSC analysis of these materials. The diffractogram of the multi-block copolymers showed a peak corresponding to the PLLA prepolymers. Taking the results of DSC and XRD together, we concluded that the crystallinity and melting of the multi-block copolymers can be attributed to the PLLA domains. Further, the multi-block copolymers consist of crystalline PLLA domains embedded in an amorphous matrix of PLLA and PDLLA-PEG-PDLLA.

3.2. Preparation of sunitinib-loaded polymeric microspheres

Sunitinib (Fig. 4) is a weak base with a p*K*a ~ 9.0 of its tertiary amine functionality [33]; the commercial product has malate as counter ion. The solubility of sunitinib malate in aqueous media (pH < 7.0) is 25 mg/ml. Sunitinib malate is only slightly soluble in DCM (<1 mg/ml) but its solubility in DMSO is rather high (40 mg/ml). In this study, sunitinib malate was loaded into microspheres via a single emulsion method using DCM as volatile solvent and DMSO as co-solvent for sunitinib malate. The morphology of sunitinib-loaded microspheres is shown in the

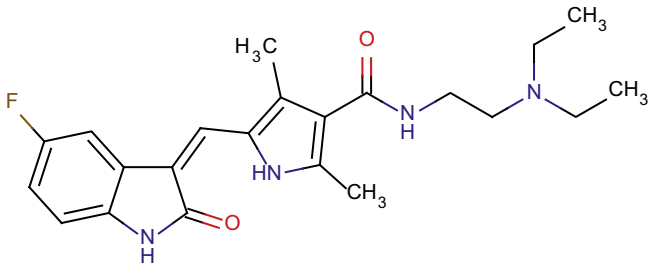

Fig. 4. Chemical structure of sunitinib. (For the interpretation of the references to color in this figure legend, the reader is referred to the web version of this article.)

SEM images (Fig. 5, left column), which illustrates that the obtained sunitinib-loaded microspheres had a smooth and non-porous surface. The particles size shown by SEM was in line with particles size acquired by Accusizer (23–34 μm). Table 2 shows the characteristics of sunitinib-loaded microspheres prepared using polymer A, B and C. The table shows that all formulations were obtained in a high yield (~80%) with average particle size ranging from 23 to 34 μm. The LE was high in microspheres based on polymer A (87%) and polymer B (73%). However, microspheres based on polymer C, the more hydrophilic polymer with highest PEG-content, showed a low LE (13%). Most likely, water absorption and swelling of microspheres during the solvent extraction resulted in higher sunitinib diffusion into the external water phase. This was confirmed by analysis of non-encapsulated sunitinib in the external phase after centrifugation of the particles, which accounted for 80% of the drug added in the emulsified organic phase with polymer C. Another factor that has contributed to the higher sunitinib loading efficiency of microspheres prepared with polymer A is the relative higher molecular weight of this polymer (Table 1), and hence the higher viscosity of the organic phase of polymer A which prevented loss of the drug before solidification of the microparticles [34].

As can be deduced from the titration curve of sunitinib, its log*D* increases from 0.9 at pH 7.0 to 2.6 at pH 9.0 (Fig. S5). Partitioning of the uncharged form sunitinib into the polymeric droplets phase is hence favored at the conditions used for emulsifying the organic phase. In contrast, the counter ion malate is charged at the studied pH values, thus resulting in encapsulation of sunitinib free base in the microparticles rather than the sunitinib malate salt. This behavior is in agreement with the encapsulation of imatinib mesylate in PLGA microparticles [35]. While imatinib base was efficiently encapsulated (70% LE) at pH 9.0, the hydrophilic mesylate anion was largely lost (<5% LE).

3.3. In-vitro degradation of sunitinib-loaded microspheres

Sunitinib-loaded microspheres based on the different multi-block copolymers (A, B and C) were incubated at 37 °C in PBS to study polymer degradation and particle erosion. SEM images showed that sunitinib-loaded microspheres, especially microspheres based on polymer A retained their spherical shape even after 210 days of incubation (Fig. 5, right panel). In contrast, the particles of polymer B and polymer C showed extensive erosion after 210 days. These observations are in line with degradation data as shown in Fig. 6. Fig. 6A shows the percentage decrease in the M_w of the polymers in time. In the first week of incubation the decrease in the M_w was 25%, 30% and 40% for polymer A, B and C, respectively, and subsequently the M_w gradually decreased in time for all polymers types. Fig. 6B shows the percentage decrease in dry mass versus time for the same particles. The dry mass of microspheres based on polymer A and B did not change during the first 60 and 30 days of incubation, respectively. Thereafter continuous weight loss was observed for both formulations. Microspheres based on polymer C showed about 20% decrease in dry mass after incubation for one week. The weight loss proceeded till the end of this experiment. The remaining mass after 210 days was 61%, 42% and 43% for microspheres based on polymer A, B and C, respectively. It can be concluded that increasing the soft PDLA-PEG-PDLA block increases the degradation rate of this type of multi-block copolymers.

To investigate the composition of degrading microspheres in time, their PEG-content was analyzed using ^{1}H NMR analysis (Fig. 6C). While the PEG-content of microspheres prepared with polymer A remained constant for more than 150 days, the other two formulations gradually showed a decrease in PEG-content. It can be expected that microspheres with higher PEG-content

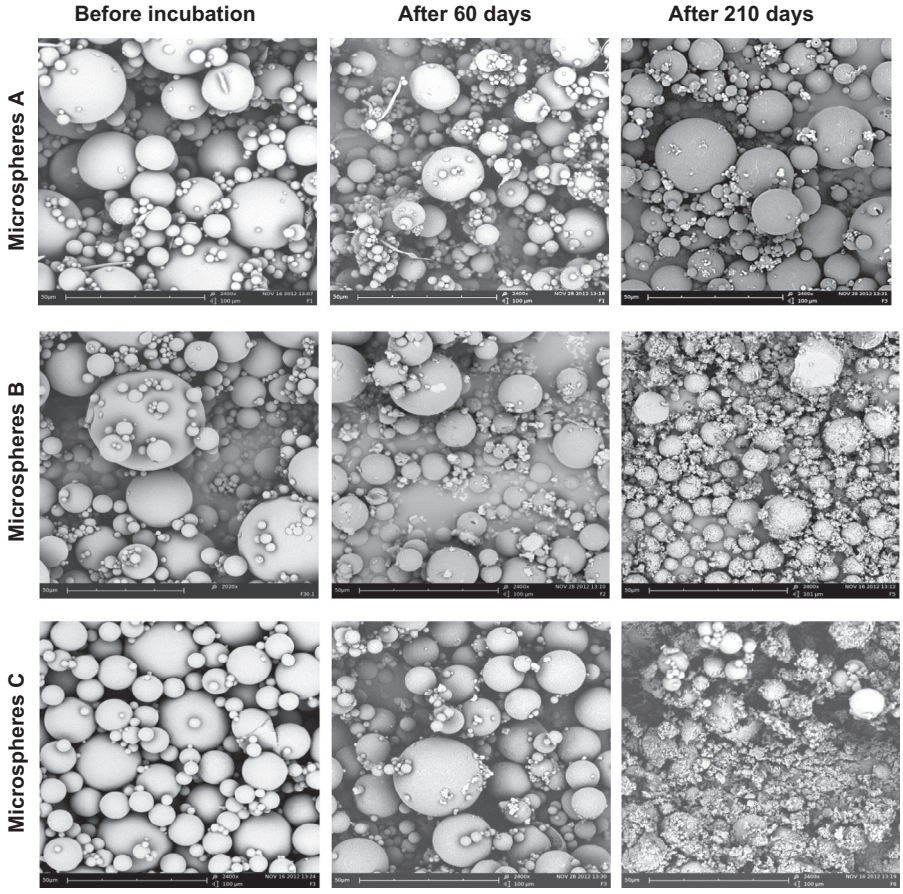

Fig. 5. SEM images of sunitinib-loaded microspheres (A, B and C) before and after incubation (60 and 120 days) in PBS pH 7.4, 37 °C.

Table 2
Characteristics of sunitinib-loaded microspheres prepared with polymer A, B and C. The concentration of polymer in DCM was 23% (w/w). The microspheres were prepared with the external water phase of pH 9.0 for 40 min and a theoretical drug loading of 0.49% (w/w). Data are expressed as mean ± SD (n = 3).

Formulation	Polymer	Yield[a] (%)	Particle size[b] (μm)	LC[c] (mg drug/g)	LE[d] (%)	Non-encapsulated drug[e] (%)
1	A	80 ± 2	26 ± 4	3.2 ± 0.5	87 ± 13	9 ± 5
2	B	87 ± 5	34 ± 3	2.7 ± 0.6	73 ± 15	24 ± 9
3	C	76 ± 5	23 ± 4	0.5 ± 0.3	13 ± 7	80 ± 3

[a] Yield of sunitinib-loaded microspheres.
[b] Particle size expressed as volume weighted mean diameter.
[c] Loading capacity expressed as sunitinib free base.
[d] Loading efficiency expressed as sunitinib free base.
[e] Percentage of sunitinib recovered in the water phase after centrifugation.

initially swell to a greater extent than microspheres based on lower PEG-content resulting in higher water absorption and hydrolysis [36]. In the initial phase of degradation (i.e. till 30 days) microspheres based on polymer C with higher PEG-content indeed showed higher degradation (decrease in M_w, dry mass and PEG-content) compared to other formulations. At day 30 of degradation the PEG-content of microspheres based on polymer C and B became similar (~8%). Thereafter, their degradation (decrease in the PEG-contents, M_w and dry mass) proceeded in the same manner. The initial loss of the PEG blocks observed in our study is in agreement with other studies reporting that the ester bonds connecting PEG and aliphatic polyester are more susceptible to hydrolysis [37,38]. In the previous study of Samadi et al., the PEG was fully removed within 5 days from the prepared nanospheres based on blends of hydroxylated aliphatic polyester, poly(D,L-lactic-co-glycolic-co-hydroxymethyl glycolic acid) (PLGHMGA) and PEG-PLGHMGA block copolymers. The relatively faster shedding of PEG from PEG-PLGHMGA systems as compared to our study can be due to both smaller particle size and greater hydrophilicity of the PLGHMGA matrix causing faster hydrolysis of the PEG-PLGHMGA ester bonds both at the surface and within the matrix [38].

The thermal properties of the degraded microspheres were analyzed by DSC (Fig. 7, Figs. S6–8 and Table S7). Fig. 7A shows that during the first week of incubation the T_g of microspheres based on polymer A remained unchanged (50 °C), but the T_g of microspheres based on polymer B and C increased from 42 °C and 35 °C to 46 °C and 45 °C, respectively. This increase in T_g can be attributed to the loss of PEG during the initial phase of degradation which is substantiated by ^{1}H NMR analysis (Fig. 6C).

The melting points and enthalpies of sunitinib-loaded microspheres did not change till 150 days of incubation (Fig. 7A and Table S7). The melting points thereafter (150 days) decreased from 138 °C, 131 °C, and 131 °C to 133 °C, 103 °C and 104 °C for

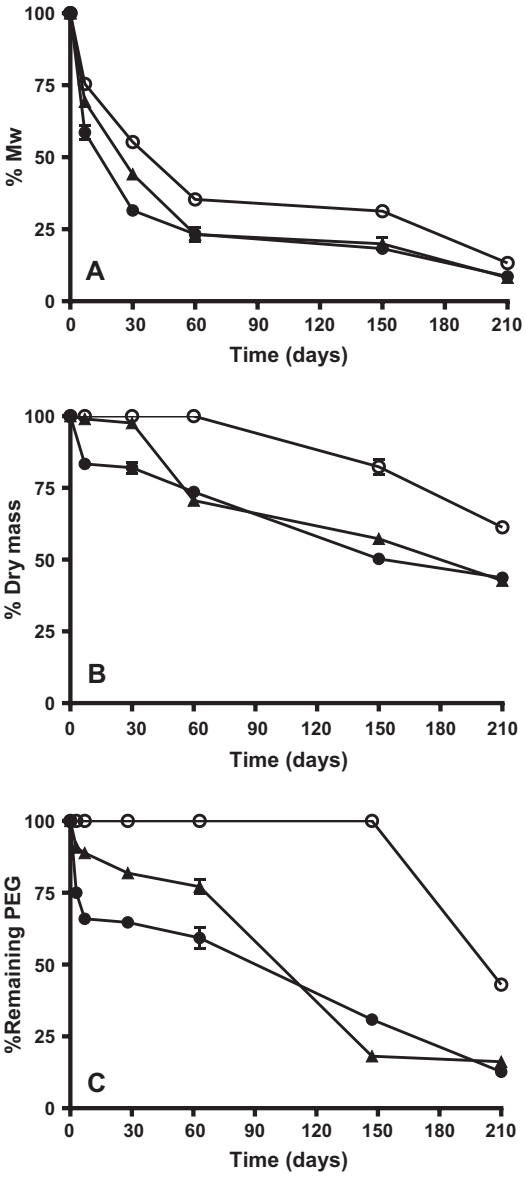

Fig. 6. Degradation of sunitinib-loaded microspheres based on different multi-block copolymers. Polymer A (open circles), polymer B (closed triangles) and polymer C (closed circles). (A) Shows changes in the M_w (%) versus time, (B) shows dry mass loss versus time and (C) shows the percentage of PEG (based on ^{1}H NMR analysis) of the same formulations after incubation in PBS pH 7.4, 37 °C for a period of 210 days, respectively. Data are expressed as mean ± SD (n = 3).

microspheres based on polymer A, B and C, respectively. The melting enthalpy increased from 26 (J/g) to 42 (J/g) for microspheres based on polymer B and C which pointed to an increased crystallinity of these polymers [39]. The observed increase in the crystallinity of the polymers can be explained by decreased molecular weight of the copolymers during degradation which gives freedom to the shorter polymer chains to rearrange and crystallize [40–42]. As mentioned above, the melting point is due to the semi-crystalline PLLA block which is more resistant to degradation than soft blocks since it is difficult for water molecules to penetrate into the crystalline domains [39]. However, as the degradation proceeded, the polymer chains became shorter which caused a decrease in the melting point [30].

Taking the results of GPC, DSC and ^{1}H NMR together, it can be concluded that an increase in the soft block content from 10% to 30% resulted in faster degradation of semi-crystalline multi-block copolymers.

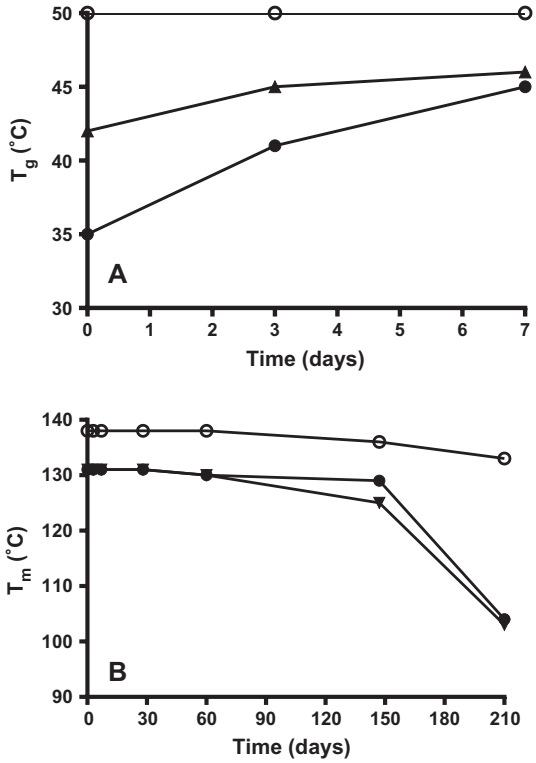

Fig. 7. Changes in polymer characteristics during degradation of sunitinib-loaded microspheres. Fig. 6A shows changes in the T_g (°C) of microspheres based on polymer A (open circles), polymer B (triangles) and polymer C (closed circles) during first week of incubation. Fig. 6B shows changes in the T_m (°C) of the same formulations after incubation in PBS pH 7.4, 37 °C for a period of 210 days, respectively. Data are expressed as mean ± SD (n = 3).

3.4. In-vitro release of sunitinib from microspheres

Sunitinib-loaded microspheres prepared with the different polymers (A, B and C) were incubated at 37 °C in PBS to study their release characteristics. Fig. 8 shows that the release profile was largely influenced by the percentage of the hydrophilic PDLA-PEG-PDLA block in the copolymers. While sunitinib release from microspheres type B and C showed a sigmoidal profile that reached complete release after about 150 days, the microspheres with 5% PEG (type A) showed a zero order release profile that reached about 30% of the encapsulated drug at the end of the incubation period of 210 days. The initial burst (release in 24 h) was 5%, 7% and 37% for microspheres based on polymer A, B and C, respectively. Fitting constants of the release profiles are summarized in Table 3. The linear fitted release of microspheres type A showed a release constant of 0.16% for 210 days and good agreement between theory and experiment was obtained (R^2 0.9767). In view of the complex processes that contributed to drug release, the release profiles of the other two curves were only poorly fitted by mechanistic models like the Korsmeyer–Peppas model. We therefore used a sigmoidal mathematical model for non-linear curve fitting according to Duvvuri et al. [27]. In this empirical model for sigmoidal drug release, constants A and B represent the relative proportion of drug release during phase I and phase III of the curves, T_{50} represents the time point at which 50% of the drug has been released and time constants k_1 and k_2 reflect the drug release rate during phase I and phase III due to diffusion and diffusion plus polymer degradation, respectively. The higher release rate in the last stage of the sigmoidal curves reflects a combination of particle erosion and the higher diffusion rate of sunitinib upon polymer degradation, but also other factors like increased

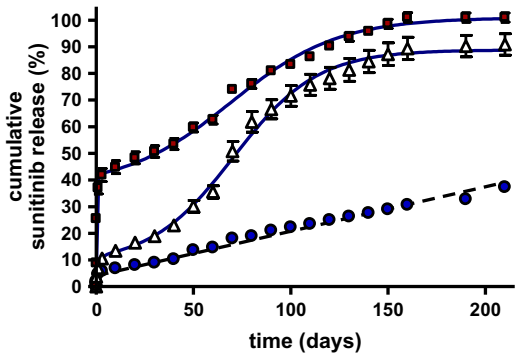

Fig. 8. *In-vitro* release study of sunitinib from microspheres in PBS, 37 °C. Blue circles represent microspheres prepared by polymer A, triangles show microspheres based on polymer B and red squares show microspheres based on polymer C. Lines drawn represent linear fit for curve A and non-linear regression fit according to Eq. (2) of curves B and C. Data are expressed as mean ± SD ($n = 3$). (For the interpretation of the references to color in this figure legend, the reader is referred to the web version of this article.)

Table 3
Best-fit values of cumulative drug release from sunitinib-loaded microspheres. Microspheres A are fitted with the zero-order model (Eq. (1)) and a sigmoidal non-linear model (Eq. (2)) while microspheres B and C are only fitted with the sigmoidal non-linear model (Eq. (2)). Corresponding curves are shown in Fig. 8.

	Fitted parameters	Microspheres A	Microspheres B	Microspheres C
Zero-order model (Eq. (1))	A	4.1 ± 0.6		
	k	0.17 ± 0.01		
	R^2	0.9767		
Sigmoidal model (Eq. (2))	A (% release)	5.3 ± 1.3	8.7 ± 2.8	37.3 ± 1.9
	k_1 (day^{-1})	0.33 ± 0.21	0.61 ± 0.50	9.42 ± 1.34
	B (% release)	30.6 ± 2.0	80.1 ± 3.4	63.6 ± 2.5
	k_2 (day^{-1})	0.026 ± 0.002	0.046 ± 0.004	0.036 ± 0.003
	T_{50} (day)	94.0 ± 5.8	70.7 ± 2.4	69.2 ± 2.5
	R^2	0.9590	0.9804	0.9883

solubility of the drug due to water influx [39,43]. This water uptake will lead to a swollen polymer matrix from which sunitinib can be released. Microspheres based on polymer A showed slower release due to their higher hydrophobicity compared to microspheres based on polymer B and C.

A more mechanistic understanding of the processes that contributed to sunitinib release was deduced from the data on *in-vitro* degradation of the microspheres (as discussed in Section 3.3). The release from microspheres A was mainly governed by diffusion till the start of particle erosion (60 days). Thereafter, sunitinib was released by a combination of diffusion and particle erosion. Sunitinib release from microspheres based on polymer B was governed by diffusion till day 30 at which time particle erosion started. Since the dry mass loss was faster as compared to polymer A, the drug release was faster till day 90. After day 90, the drug release became slower which can be explained by reduction in the PEG-content and increasing crystallinity which in turn increases the hydrophobicity of the microspheres, in agreement with degradation data.

When a low molecular weight drug is molecularly dispersed in the polymer, its release will be governed by diffusion although the degradation of the matrix may help in liberating the loaded drug. On the other hand, if the drug is crystallized in the polymer, the release will be governed by degradation. The drug may also release by diffusion through the polymer if the degradation is slow or the drug has some solubility in the polymeric matrix [44,45]. Since the loading capacity of sunitinib-loaded microspheres is below the detection limits of DSC and XRD (<0.5%), we could not confirm the physical state (amorphous or crystalline) of sunitinib in the microspheres. Nonetheless, sunitinib solubilization may play a rule in drug release from microparticles. Taking the results of degradation and release study together, it can be concluded that sunitinib released from the microspheres by a combination of diffusion through the soft blocks and polymer erosion. The release rate could be tailored by controlling the PEG-containing soft block content of the final multi-block copolymers.

3.5. Anti-angiogenic effect of sunitinib-loaded microspheres

The chick embryo chorioallantoic membrane (CAM) is an extraembryonic membrane responsible for mediating gas and nutrient exchanges until hatching. Since it has a condensed capillary network, it has been commonly used to study both angiogenesis and anti-angiogenesis processes [46]. The CAM assay is a suitable model to screen anti-angiogenic effects of various drugs before performing animal studies [47,48]. It is a suitable model to study the efficacy of drugs for the treatment of age-related macular degeneration [49–52]. We have placed a ring on top of the CAM membrane to keep the administered drugs in place. However, this ring does not avoid uptake of the drug into the CAM and subsequent diffusion of the drug into the egg white. Hence, the locally administered drug can dilute into the total distribution volume of the egg white and egg yellow, similar to drug transport that can be expected upon injection of drugs into the human eye.

In this study both sunitinib malate and sunitinib-loaded microspheres suspended in PBS, were applied on the CAM to study their anti-angiogenic effect. The number of blood vessels before and 24 h after drug exposure was compared (Fig. 9). The sunitinib-microspheres based on polymer B were used, since this formulation combined good loading efficiency with a prolonged release profile without extensive burst release. Fig. 9A shows that both the control groups (30 µl vehicle, PBS or 0.5 mg of blank microspheres) and sunitinib (50 ng/egg) did not change the number of blood vessels compared to 24 h before applying the drug or vehicle. On the other hand, by increasing the dose of sunitinib to 100 ng/egg the number of blood vessels significantly reduced (paired t-test, ($p < 0.05$) compared to 24 h before applying the drug. To study the anti-angiogenic potential of sunitinib-loaded microspheres, we administered 0.5 mg microspheres type B suspended in 30 µl PBS onto the CAM. This amount of microspheres corresponded to a dose of 1350 ng sunitinib and an expected release of 65 ng sunitinib/day based on the fitted release profile of microspheres B. We observed a pronounced decrease in the number of blood vessels as compared to 24 h before applying the microspheres ($p < 0.05$). One may expect a higher anti-angiogenic effect for the free drug than the drug-loaded microspheres as the free drug is available for 24 h while sunitinib microspheres release their payload gradually. In contrast to the free drug, which is fully dissolved at the moment of its pipetting onto the CAM, drug-loaded microspheres actually require a drug release phase before the dissolved molecules can exert their inhibitory activity in the CAM, or before they can diffuse further into the egg. Hence, one can expect differences in the temporal distribution of the drug between free drug and drug-loaded microspheres.

The pronounced anti-angiogenic effect clearly illustrates that sunitinib-loaded microspheres have potential for suppressing angiogenesis in a localized compartment and that the bioactivity of the drug is preserved after releasing from microspheres which was also confirmed by HPLC analysis of the released drug (Fig. S9).

In this study, the LC of sunitinib microspheres was rather low; this mainly is due to low solubility of sunitinib in the organic phase used for emulsification of the microparticles. However, sunitinib is

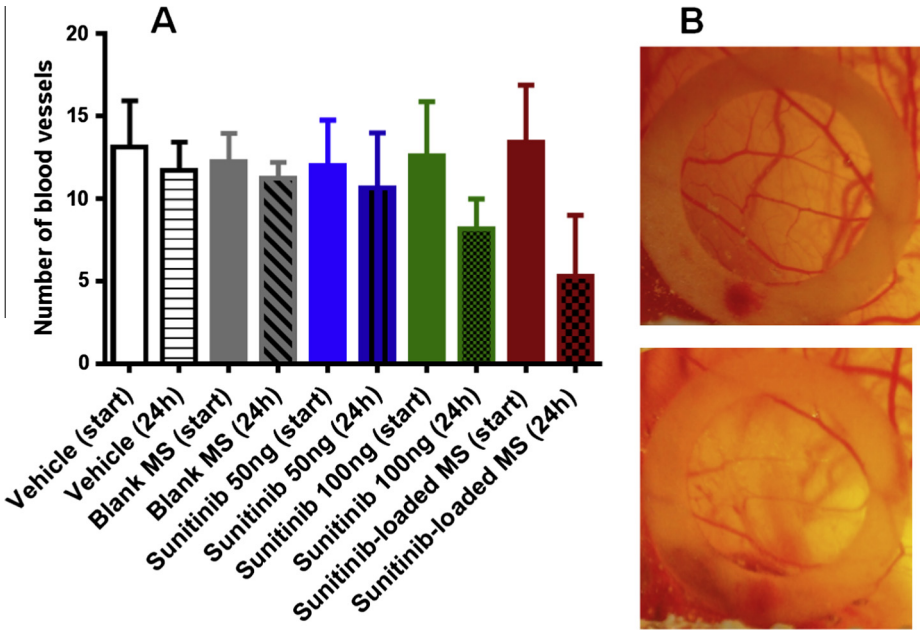

Fig. 9. Inhibition of angiogenesis in the CAM assay. (A) Shows the number of blood vessels before (bars without stripes or hatches) and 24 h after administration of compounds on CAM (striped or hatched bars). From left to right: vehicle solution (PBS), 0.5 mg blank microspheres, 50 ng sunitinib, 100 ng sunitinib and 0.5 mg sunitinib-loaded microspheres based on polymer B. (B) Representative pictures of chorioallantoic membrane before (upper figure) and 24 h (lower figure) after applying of sunitinib-loaded microspheres. Data are expressed as mean ± SD (n = 6). (For the interpretation of the references to color in this figure legend, the reader is referred to the web version of this article.)

a highly potent receptor tyrosine kinase inhibitor and only relative low levels (nanomolar concentrations) are needed to exert inhibition of $VEGFR_2$ in endothelial cells [53]. Moreover, the eye is a confined compartment and local release of sunitinib within the eye may result in sufficient levels of the released drug.

The microparticles described in this study are made of relatively hydrolytically degradable polymers that showed good biocompatibility when used as polymeric coated stent delivery systems [54]. Hence, we expect good biocompatibility for this type of microspheres after intravitreal injection, although further studies addressing their safety after ocular delivery are required to corroborate this. Moreover, local application of sunitinib microspheres in the eye in appropriate animal models of ocular neovascularization should demonstrate long term anti-angiogenic activity, in correlation to the sustained release profiles observed in this paper. While VEGF antagonists have revolutionized the treatment of ocular neovascularization, there is still substantial room for improvement. In animal models, combined blockade of VEGF and PDGF-B showed greater benefit than blockade of VEGF alone [55,56]. Sunitinib malate is a multi-targeted receptor tyrosine kinase inhibitor blocking both VEGF and PDGF receptors. Sunitinib showed more potent inhibitory effect compared to bevacizumab which only inhibits VEGF in some preclinical studies. Ocular delivery of sunitinib may therefore be an attractive approach for treatment of ocular neovascularization.

4. Conclusion

In the current investigation, we have developed sunitinib loaded [PDLLA-PEG-PDLLA]-*b*-[PLLA] microspheres which continuously release the multikinase inhibitor for over 30 weeks by a combination of diffusion through the soft blocks and polymer erosion. Sunitinib microspheres showed antiangiogenic effect in a CAM assay and may be a promising delivery system for long-term suppression of neovascularization by intravitreal injection.

Conflict of interest

Authors declare that there is no conflict of interest in this work.

Acknowledgments

The authors would like to thank E.H.E. Pieters, M.J. Van Steenbergen and M. Versluijs for their technical assistance in CAM assay, DSC and X-ray study, respectively. This work is partly granted by the Iranian Ministry of Health and Medical Education.

Appendix A. Supplementary material

Supplementary data associated with this article can be found, in the online version, at http://dx.doi.org/10.1016/j.ejpb.2015.02.011.

References

[1] M.R. Barakat, P.K. Kaiser, VEGF inhibitors for the treatment of neovascular age-related macular degeneration, Expert Opin. Investig. Drugs 18 (2009) 637–646.
[2] A.L. Daugherty, L.K. Rangell, R. Eckert, J. Zavala-Solorio, F. Peale, R.J. Mrsny, Sustained release formulations of rhVEGF(1)(6)(5) produce a durable response in a murine model of peripheral angiogenesis, Eur. J. Pharm. Biopharm. 78 (2011) 289–297.
[3] P.J. Rosenfeld, D.M. Brown, J.S. Heier, D.S. Boyer, P.K. Kaiser, C.Y. Chung, R.Y. Kim, MARINA Study Group, Ranibizumab for neovascular age-related macular degeneration, N. Engl. J. Med. 355 (2006) 1419–1431.
[4] Q.T. Ho, C.J. Kuo, Vascular endothelial growth factor: biology and therapeutic applications, Int. J. Biochem. Cell Biol. 39 (2007) 1349–1357.
[5] J.W. Miller, J. Le Couter, E.C. Strauss, N. Ferrara, Vascular endothelial growth factor A in intraocular vascular disease, Ophthalmology 120 (2013) 106–114.
[6] J. Welti, S. Loges, S. Dimmeler, P. Carmeliet, Recent molecular discoveries in angiogenesis and antiangiogenic therapies in cancer, J. Clin. Invest. 123 (2013) 3190–3200.
[7] P. Maier, A.S. Unsoeld, B. Junker, G. Martin, J. Drevs, L.L. Hansen, H.T. Agostini, Intravitreal injection of specific receptor tyrosine kinase inhibitor PTK787/ZK222 584 improves ischemia-induced retinopathy in mice, Graefes Arch. Clin. Exp. Ophthalmol. 243 (2005) 593–600.
[8] S.A. Vinores, Pegaptanib in the treatment of wet, age-related macular degeneration, Int. J. Nanomed. 1 (2006) 263–268.

[9] L. Wood, Sunitinib malate for the treatment of renal cell carcinoma, Expert Opin. Pharmacother. 13 (2012) 1323–1336.
[10] B. Detry, S. Blacher, C. Erpicum, J. Paupert, L. Maertens, C. Maillard, C. Munaut, N.E. Sounni, V. Lambert, J.M. Foidart, J.M. Rakic, D. Cataldo, A. Noel, Sunitinib inhibits inflammatory corneal lymphangiogenesis, Invest. Ophthalmol. Vis. Sci. 54 (2013) 3082–3093.
[11] R. Cao, L.D. Jensen, I. Soll, G. Hauptmann, Y. Cao, Hypoxia-induced retinal angiogenesis in zebrafish as a model to study retinopathy, PLoS ONE 3 (2008) e2748.
[12] H. Takahashi, R. Obata, Y. Tamaki, A novel vascular endothelial growth factor receptor 2 inhibitor, SU11248, suppresses choroidal neovascularization in vivo, J. Ocul. Pharmacol. Ther. 22 (2006) 213–218.
[13] R.J. Motzer, S. Hoosen, C.L. Bello, J.G. Christensen, Sunitinib malate for the treatment of solid tumours: a review of current clinical data, Expert Opin. Investig. Drugs 15 (2006) 553–561.
[14] M.L. Telli, R.M. Witteles, G.A. Fisher, S. Srinivas, Cardiotoxicity associated with the cancer therapeutic agent sunitinib malate, Ann. Oncol. 19 (2008) 1613–1618.
[15] M.E. Dolman, S. Harmsen, G. Storm, W.E. Hennink, R.J. Kok, Drug targeting to the kidney: advances in the active targeting of therapeutics to proximal tubular cells, Adv. Drug Deliv. Rev. 62 (2010) 1344–1357.
[16] S. Akhter, F. Ramazani, M.Z. Ahmad, F.J. Ahmad, Z. Rahman, A. Bhatnagar, G. Storm, Ocular pharmacoscintigraphic and aqueous humoral drug availability of ganciclovir-loaded mucoadhesive nanoparticles in rabbits, Eur. J. Nanomed. 5 (2013) 159–166.
[17] A. Sabzevari, K. Adibkia, H. Hashemi, A. Hedayatfar, N. Mohsenzadeh, F. Atyabi, M.H. Ghahremani, R. Dinarvand, Polymeric triamcinolone acetonide nanoparticles as a new alternative in the treatment of uveitis: in vitro and in vivo studies, Eur. J. Pharm. Biopharm. 84 (2013) 63–71.
[18] S.S. Shah, L.V. Denham, J.R. Elison, P.S. Bhattacharjee, C. Clement, T. Huq, J.M. Hill, Drug delivery to the posterior segment of the eye for pharmacologic therapy, Expert Rev. Ophthalmol. 5 (2010) 75–93.
[19] M. Stankovic, J. Tomar, C. Hiemstra, R. Steendam, H.W. Frijlink, W.L. Hinrichs, Tailored protein release from biodegradable poly(epsilon-caprolactone-PEG)-b-poly(epsilon-caprolactone) multiblock-copolymer implants, Eur. J. Pharm. Biopharm. 87 (2014) 329–337.
[20] M. Stankovic, H. de Waard, R. Steendam, C. Hiemstra, J. Zuidema, H.W. Frijlink, W.L. Hinrichs, Low temperature extruded implants based on novel hydrophilic multiblock copolymer for long-term protein delivery, Eur. J. Pharm. Sci. 49 (2013) 578–587.
[21] M. Gillissen, R. Steendam, A. van der Laan, E. Tijsma, Development of doxycycline-eluting delivery systems based on SynBiosys™ biodegradable multi-block copolymers, J. Control. Release 116 (2006) e90–e92.
[22] L.L. Falke, S.H. van Vuuren, F. Kazazi-Hyseni, F. Ramazani, T.Q. Nguyen, G.J. Veldhuis, E.M. Maarseveen, J. Zandstra, J. Zuidema, L.F. Duque, R. Steendam, E.R. Popa, R.J. Kok, R. Goldschmeding, Local therapeutic efficacy with reduced systemic side effects by rapamycin-loaded subcapsular microspheres, Biomaterials 42 (2015) 151–160.
[23] C. Chaw, C. Tan, Y. Yang, L. Wang, S. Moochhala, Design of physostigmine-loaded polymeric microparticles for pretreatment against exposure to organophosphate agents, Biomaterials 24 (2003) 1271–1277.
[24] R. Bodmeier, J.W. McGinity, Solvent selection in the preparation of poly(DL-lactide) microspheres prepared by the solvent evaporation method, Int. J. Pharm. 43 (1988) 179–186.
[25] A. Göpferich, Mechanisms of polymer degradation and erosion, Biomaterials 17 (1996) 103–114.
[26] M.E. Dolman, S. Harmsen, E.H. Pieters, R.W. Sparidans, M. Lacombe, B. Szokol, L. Orfi, G. Keri, G. Storm, W.E. Hennink, R.J. Kok, Targeting of a platinum-bound sunitinib analog to renal proximal tubular cells, Int. J. Nanomed. 7 (2012) 417–433.
[27] S. Duvvuri, K. Gaurav Janoria, A.K. Mitra, Effect of polymer blending on the release of ganciclovir from PLGA microspheres, Pharm. Res. 23 (2006) 215–223.
[28] I. Rashkov, N. Manolova, S.M. Li, J.L. Espartero, M. Vert, Synthesis, characterization, and hydrolytic degradation of PLA/PEO/PLA triblock copolymers with short poly(L-lactic acid) chains, Macromolecules 29 (1996) 50–56.
[29] U.W. Gedde, Polymer Physics, Chapman & Hall, London, New York, 1995.
[30] S.J. de Jong, W.N.E. van Dijk-Wolthuis, J.J. Kettenes-van den Bosch, P.J.W. Schuyl, W.E. Hennink, Monodisperse enantiomeric lactic acid oligomers: preparation, characterization, and stereocomplex formation, Macromolecules 31 (1998) (American Chemical Society).
[31] Inkinen, From lactic acid to poly(lactic acid) (PLA): characterization and analysis of PLA and its precursors, Biomacromolecules 12 (2011) 523–532.
[32] V.T. Tran, J.P. Karam, X. Garric, J. Coudane, J.P. Benoit, C.N. Montero-Menei, M.C. Venier-Julienne, Protein-loaded PLGA-PEG-PLGA microspheres: a tool for cell therapy, Eur. J. Pharm. Sci. 45 (2012) 128–137.
[33] K.J. Gotink, H.J. Broxterman, M. Labots, R.R. de Haas, H. Dekker, R.J. Honeywell, M.A. Rudek, L.V. Beerepoot, R.J. Musters, G. Jansen, A.W. Griffioen, Y.G. Assaraf, R. Pili, G.J. Peters, H.M. Verheul, Lysosomal sequestration of sunitinib: a novel mechanism of drug resistance, Clin. Cancer Res. 17 (2011) 7337–7346.
[34] Y. Yeo, K. Park, Control of encapsulation efficiency and initial burst in polymeric microparticle systems, Arch. Pharm. Res. 27 (2004) 1–12.
[35] F. Ramazani, W. Chen, C.F. Van Nostrum, G. Storm, F. Kiessling, T. Lammers, W.E. Hennink, R.J. Kok, Formulation and characterization of microspheres loaded with imatinib for sustained delivery, Int. J. Pharm. (2015), http://dx.doi.org/10.1016/j.ijpharm.2015.01.043.
[36] J.D. Clapper, J.M. Skeie, R.F. Mullins, C.A. Guymon, Development and characterization of photopolymerizable biodegradable materials from PEG–PLA–PEG block macromonomers, Polymer 48 (2007) 6554–6564.
[37] J.M. Bezemer, D.W. Grijpma, P.J. Dijkstra, C.A. van Blitterswijk, J. Feijen, A controlled release system for proteins based on poly(ether ester) block-copolymers: polymer network characterization, J. Control. Release 62 (1999) 393–405.
[38] N. Samadi, M.J. van Steenbergen, J.B. van den Dikkenberg, T. Vermonden, C.F. van Nostrum, M. Amidi, W.E. Hennink, Nanoparticles based on a hydrophilic polyester with a sheddable PEG coating for protein delivery, Pharm. Res. 31 (2014) 2593–2604.
[39] L. Youxin, C. Volland, T. Kissel, In-vitro degradation and bovine serum albumin release of the ABA triblock copolymers consisting of poly (L(+) lactic acid), or poly(L(+) lactic acid-co-glycolic acid) A-blocks attached to central polyoxyethylene B-blocks, J. Control. Release 32 (1994) 121–128.
[40] Su Ming Li, H. Garreau, M. Vert, Structure-property relationships in the case of the degradation of massive poly(α-hydroxyacids) in aqueous media, J. Mater. Sci. – Mater. Med. 1 (1990) 131–139.
[41] M. Vert, S. Li, H. Garreau, More about the degradation of LA/GA-derived matrices in aqueous media, J. Control. Release 16 (1991) 15–26.
[42] M. Therin, P. Christel, S. Li, H. Garreau, M. Vert, In vivo degradation of massive poly(alpha-hydroxy acids): validation of in vitro findings, Biomaterials 13 (1992) 594–600.
[43] E. Kang, J. Robinson, K. Park, J. Cheng, Paclitaxel distribution in poly(ethylene glycol)/poly(lactide-co-glycolic acid) blends and its release visualized by coherent anti-Stokes Raman scattering microscopy, J. Control. Release 122 (2007) 261–268.
[44] A. Gaignaux, J. Reeff, F. Siepmann, J. Siepmann, C. De Vriese, J. Goole, K. Amighi, Development and evaluation of sustained-release clonidine-loaded PLGA microparticles, Int. J. Pharm. 437 (2012) 20–28.
[45] E. D'Aurizio, C.F. van Nostrum, M.J. van Steenbergen, P. Sozio, F. Siepmann, J. Siepmann, W.E. Hennink, A. Di Stefano, Preparation and characterization of poly(lactic-co-glycolic acid) microspheres loaded with a labile antiparkinson prodrug, Int. J. Pharm. 409 (2011) 289–296.
[46] D. Ribatti, Chick embryo chorioallantoic membrane as a useful tool to study angiogenesis, Int. Rev. Cell. Mol. Biol. 270 (2008) 181–224.
[47] A. Vargas, M. Zeisser-Labouebe, N. Lange, R. Gurny, F. Delie, The chick embryo and its chorioallantoic membrane (CAM) for the in vivo evaluation of drug delivery systems, Adv. Drug Deliv. Rev. 59 (2007) 1162–1176.
[48] A. Ozcetin, A. Aigner, U. Bakowsky, A chorioallantoic membrane model for the determination of anti-angiogenic effects of imatinib, Eur. J. Pharm. Biopharm. 85 (2013) 711–715.
[49] J.H. Kim, J.H. Kim, Y.S. Yu, K.H. Park, H.J. Kang, H.Y. Lee, K.W. Kim, Antiangiogenic effect of deguelin on choroidal neovascularization, J. Pharmacol. Exp. Ther. 324 (2008) 643–647.
[50] Q. Ebrahem, K. Renganathan, J. Sears, A. Vasanji, X. Gu, L. Lu, R.G. Salomon, J.W. Crabb, B. Anand-Apte, Carboxyethylpyrrole oxidative protein modifications stimulate neovascularization: implications for age-related macular degeneration, Proc. Natl. Acad. Sci. USA 103 (2006) 13480–13484.
[51] L. Pan, J.L. Hu, W.J. Wang, X.J. Zhang, J. Wei, Z.D. Liu, Y.H. Zhang, H.M. Xu, Molecular mechanisms of (R,R)ZX-5 on NO synthesis and its anti-angiogenic effect, Int. J. Mol. Sci. 13 (2012) 2717–2726.
[52] A. Vargas, M. Eid, M. Fanchaouy, R. Gurny, F. Delie, In vivo photodynamic activity of photosensitizer-loaded nanoparticles: formulation properties, administration parameters and biological issues involved in PDT outcome, Eur. J. Pharm. Biopharm. 69 (2008) 43–53.
[53] J.C. Welti, M. Gourlaouen, T. Powles, S.C. Kudahetti, P. Wilson, D.M. Berney, A.R. Reynolds, Fibroblast growth factor 2 regulates endothelial cell sensitivity to sunitinib, Oncogene 30 (2011) 1183–1193.
[54] N.A. Lockwood, R.W. Hergenrother, L.M. Patrick, S.M. Stucke, R. Steendam, E. Pacheco, R. Virmani, F.D. Kolodgie, B. Hubbard, In vitro and in vivo characterization of novel biodegradable polymers for application as drug-eluting stent coatings, J. Biomater. Sci. Polym. Ed. 21 (2010) 529–552.
[55] K. Takahashi, Y. Saishin, Y. Saishin, A.G. King, R. Levin, P.A. Campochiaro, Suppression and regression of choroidal neovascularization by the multitargeted kinase inhibitor pazopanib, Arch. Ophthalmol. 127 (2009) 494–499.
[56] N. Jo, C. Mailhos, M. Ju, E. Cheung, J. Bradley, K. Nishijima, G.S. Robinson, A.P. Adamis, D.T. Shima, Inhibition of platelet-derived growth factor B signaling enhances the efficacy of anti-vascular endothelial growth factor therapy in multiple models of ocular neovascularization, Am. J. Pathol. 168 (2006) 2036–2053.